



# Multifunctional fluorocarbon-conjugated nanoparticles of varied morphologies to enhance diagnostic effects in breast cancer

Melissa R. Laughter, PhD, Anna Laura Nelson, MS, Maria B. Bortot, PhD, Brisa Pena, PhD, Daewon Park, PhD

1 College of Engineering and Applied Science, University of Colorado Denver | Anschutz Medical Campus | Anschutz Medical Campus, 12700 E. 19th Avenue, Research 2 – Building P15, Aurora, CO 80045-2560, USA

## Introduction

Approximately 20% of breast cancers overexpress human epidermal growth factor receptor 2 (HER2+). For these patients, the standard of care involves trastuzumab (Herceptin), an anti-HER2 monoclonal antibody. Although this drug represents a significant treatment breakthrough, there lacks a reliable method to track the efficacy and progression of treatment.

Researchers have begun utilizing mesoporous silica nanoparticles (MSNs) due to their echogenic nature and ability to enhance the diagnostic capacity of ultrasound in cancers. In this work, we propose a **trastuzumab-MSN-fluorocarbon (FC)** system to improve the diagnostic approach to HER2+ breast cancer. By comparing various MSN shapes (e.g. amorphous, spherical, and tubular) along with the conjugation of a FC, we aim to optimize both the delivery of trastuzumab and ultrasound contrast, while maximizing the diagnostic effects.

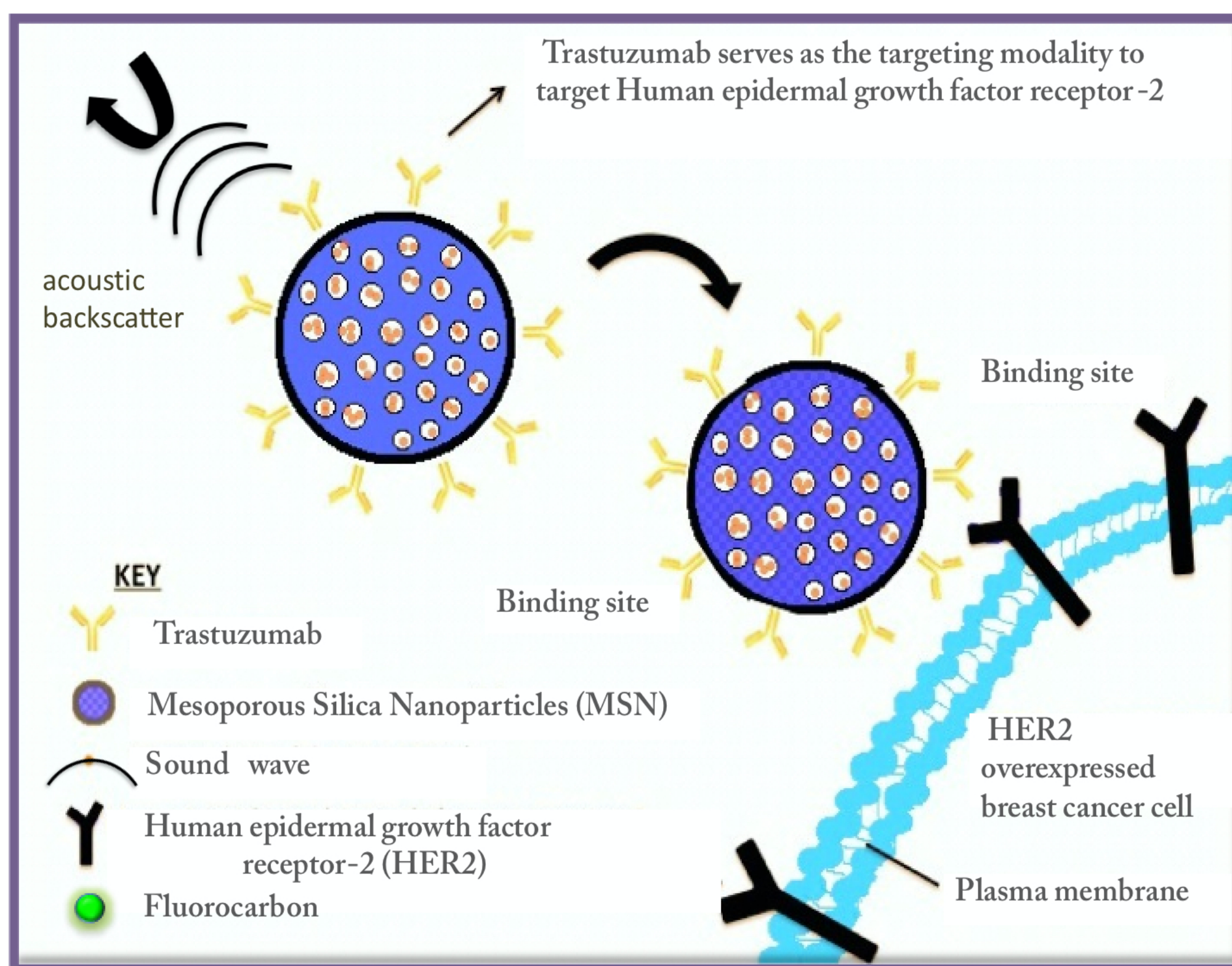


Figure 1. Schematic of proposed mechanism of action of nanoparticle system.

## Objectives

- 1) Synthesize mesoporous silica nanoparticles of varying morphologies (amorphous, spherical, and tubular).
- 2) Confirm correct morphology of MSNs through SEM.
- 3) Conjugate a fluorocarbon to the surface of each MSN.
- 4) Quantify the mean pixel intensities produced by each of the MSN.
- 5) Analyze nanoparticle attachment and endocytosis with HER2+ cells.

## Methods

### MSN Fabrication

Mesoporous silica nanoparticles are synthesized through a series of condensation reactions. Surfactant or template removal allows for the MSN to acquire a porous structure. Amorphous, tubular, and spherical MSNs were synthesized using slight variations in preparation protocols.

### Trastuzumab-MSN-fluorocarbon Fabrication

The surface of each MSN was then hydroxylated, conjugated with HDI, and finally conjugated with PEG. Next, MSN-HDI pegylated particles were conjugated with fluorocarbon and trastuzumab. Each step in this process was confirmed through FT-IR.

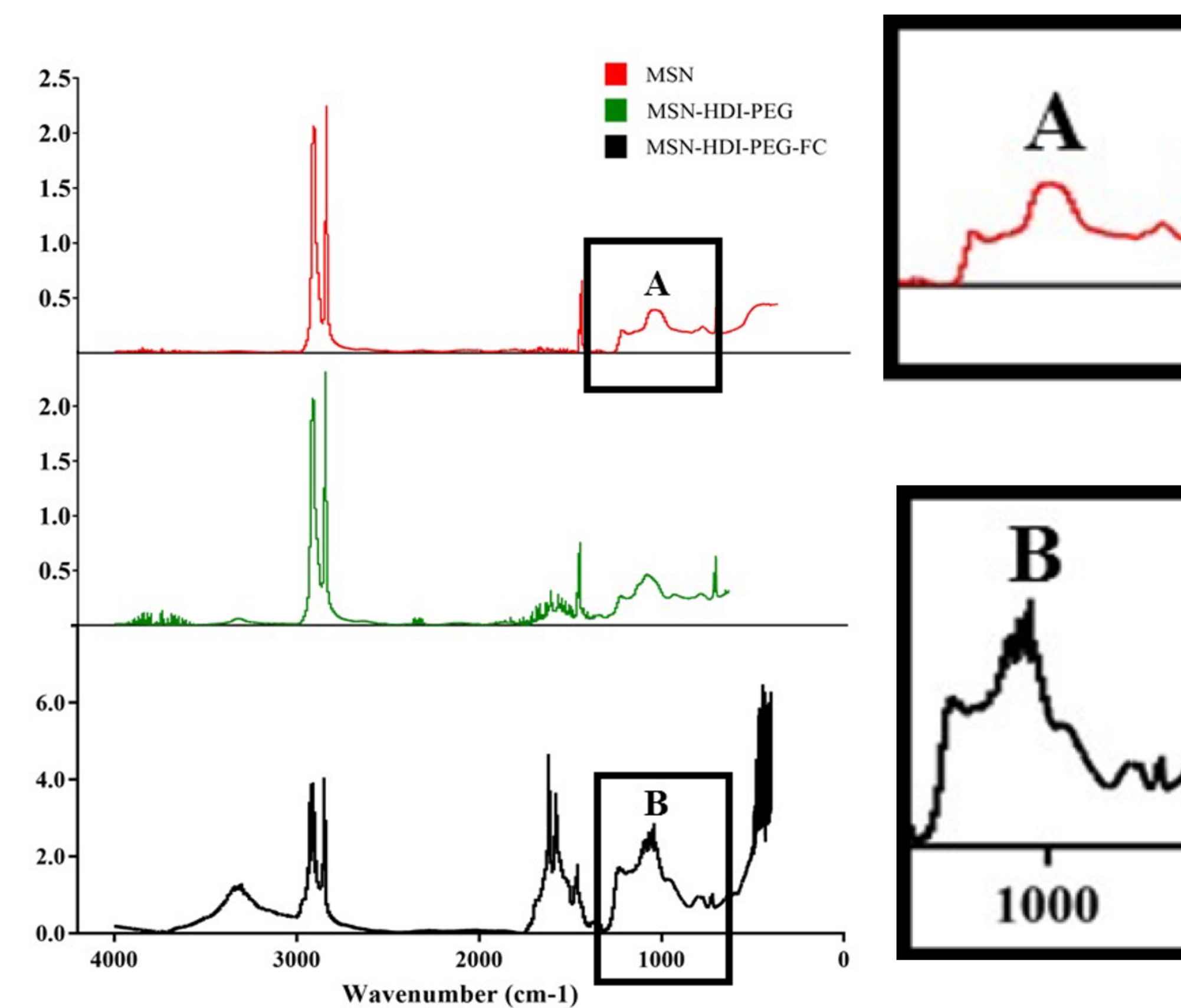


Figure 2. Fourier transform infrared (FT-IR) spectroscopy was used to confirm the successful conjugation of each moiety to the surface of the MSNs. Peak A showing Si-O-Si vibrations at 1079-1088 cm<sup>-1</sup>. Peak B showing FC stretching at 1050-1132 cm<sup>-1</sup>. Peak C showing hydroxyl group vibrations at 3378 cm<sup>-1</sup>

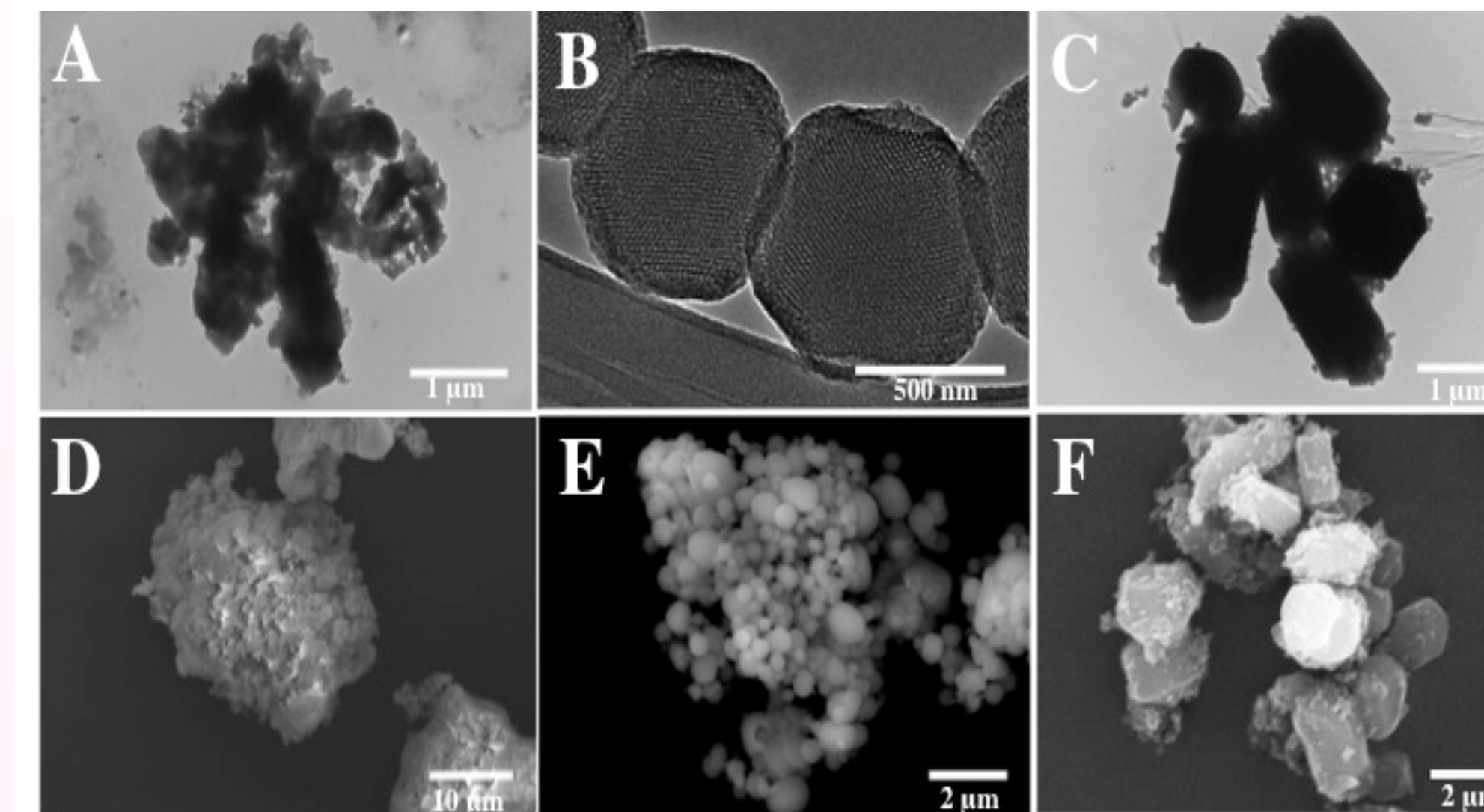
### Ultrasound pixel intensity

Single-pulse ultrasound measurements were obtained using Non-Destructive Testing (NDT) with a frequency of 6.6 MHz at a depth of 2.5 cm. MSNs dispersed at different concentrations were imaged using ultrasound and pixel intensity quantified with ImageJ.

### In-vitro HER2+ cell assay

HER2+ cells were prepared in a solution of DMEM F12 media with 10% fetal bovine serum (FBS) and 1% penicillin/streptomycin. Six experimental samples were tested: Amorphous-Herceptin, Sphere-Herceptin, Tubular-Herceptin, Amorphous-FC-Herceptin, Sphere-FC-Herceptin and Tubular-FC-Herceptin. Samples were imaged using a confocal microscope.

## Results



Zeta-Sizer Results (nm)						
	Tubular-Herceptin	Tubular	Spherical-Herceptin	Spherical	Amorphous-Herceptin	Amorphous
Average	2032.7	1148.7	2124.0	1133.7	1155.0	2374.8
Std Dev	568.4	207.9	369.7	331.6	401.7	2087.7
PDI	0.08	0.03	0.03	0.09	0.12	0.78

Figure 3. Size distribution of the various MSNs. Electron microscopy images of MSN for structural characterization analysis. Average diameter, standard deviation and PDI of MSNs through zeta-sizer.

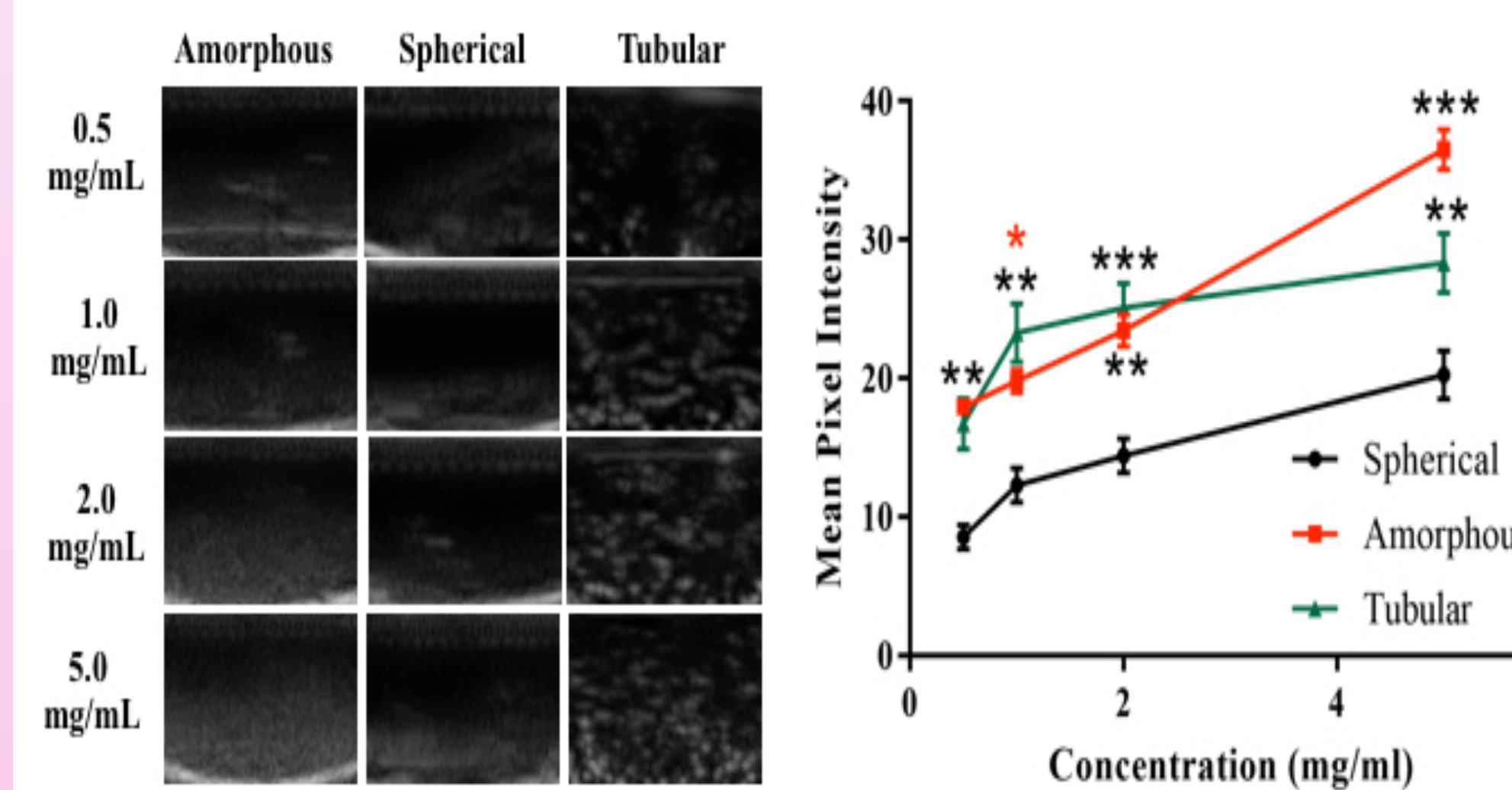


Figure 4. Ultrasound images of each nanoparticle shape (amorphous, spherical, and tubular) at various concentrations followed by analysis of mean pixel intensities of the ultrasound studies.

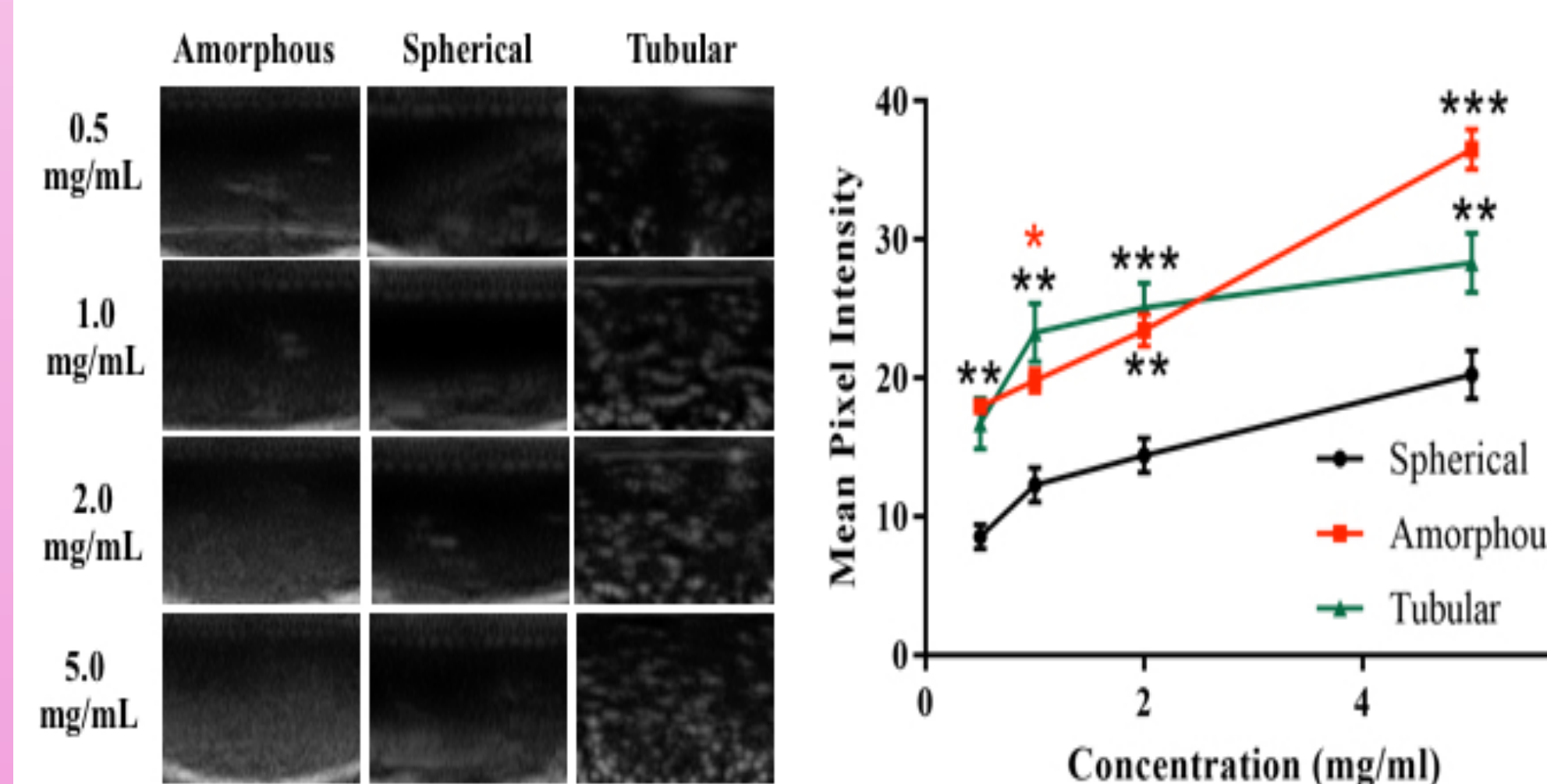


Figure 5. Ultrasound images of each nanoparticle shape (amorphous, spherical and tubular) conjugated with fluorocarbon at various concentrations followed by analysis of mean pixel intensities of the ultrasound studies.

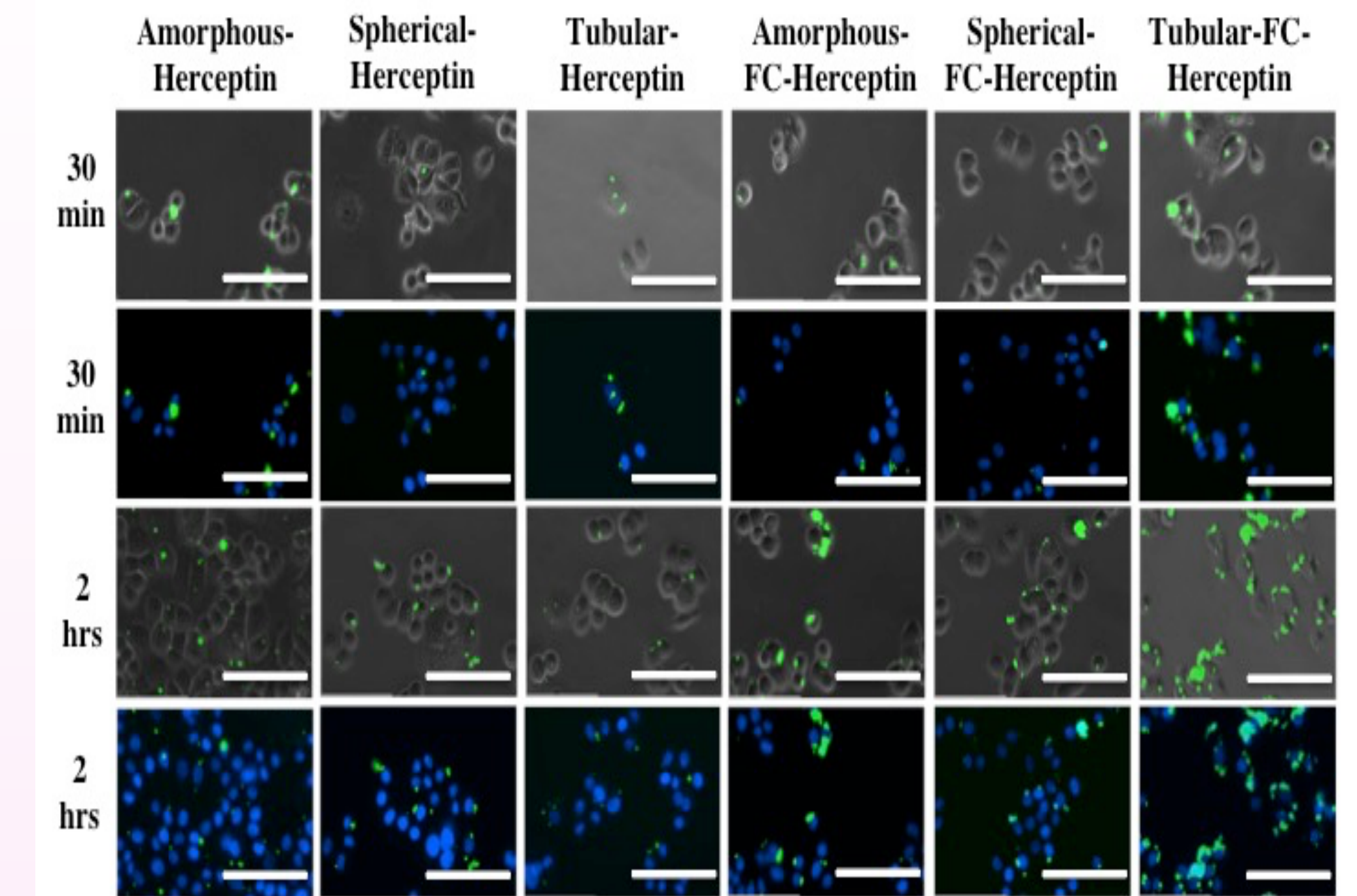


Figure 6. Fluorescent images of MSNs with and without fluorocarbon attachment incubated with HER2+ cells for 30 minutes or 2 hours. Green staining indicated the presence of fluorocarbon conjugated MSNs. Blue staining indicated DAPA staining.

## Conclusions

- 1) Fluorocarbon conjugated mesoporous silica nanoparticles produced higher mean pixel intensities.
- 2) At lower non-toxic concentrations, tubular shaped nanoparticles produced a higher mean pixel intensity compared to amorphous and spherical particles.
- 3) All systems displayed a clear binding preference toward HER2 positive breast cancer cells.
- 4) Increased incubation times and conjugation of fluorocarbon to mesoporous silica nanoparticles increased binding preference to HER2-positive cells.
- 5) The highest binding affinity was seen with tubular shaped nanoparticles compared to amorphous and spherical particles.

## References

1. Nahta, R., Esteva F. 2006. HER2 therapy: Molecular mechanisms of trastuzumab resistance. *Breast Cancer Res*, 8(6) 215.
2. Colombo, M., Corsi, F., Foschi, D., Mazantini E., Mazzucchelli, S., Morasso, C., Occhipinti, E., Polito, L., Prosperi, D., Ronchi S., Verderio, P. 2010. HER2 targeting as a two-sided strategy for breast cancer diagnosis and treatment: Outlook and recent implications in nanomedical approaches. *Pharmacological Research*, 62(2), 150-165.
3. Milgroom, A., Intrator, M., Madhavan, K., Mazzaro, L., Shandas, R., Liu, B., Park, D. 2014. Mesoporous silica nanoparticles as a breast-cancer targeting ultrasound contrast agent. *Colloids and Surfaces B: Biointerfaces*, 116(1), 652-657.
4. He, Q., Shi, J., Chen, F., Zhu, M., Zhang, L. 2010. An anticancer drug delivery system based on surfactant-templated mesoporous silica nanoparticles. *Biomaterials*, 31(12), 3335-3346.